Biophysical Chemistry, 46 (1990) 155–166
Elsevier



BIOCHE 01443

# Molecular structure of tetanus neurotoxin as revealed by Fourier transform infrared and circular dichroic spectroscopy

Bal Ram Singh [a], Michael P. Fuller [b] and Giampietro Schiavo [a,*]

[a] *Department of Food Microbiology and Toxicology, and Environmental Toxicology Center, University of Wisconsin, Madison, WI 53706 and* [b] *Nicolet Instrument Corp., Madison, WI, U.S.A.*

Received 9 October 1989
Revised manuscript received 29 December 1989
Accepted 2 January 1990

CD; Fourier transform infrared spectroscopy; pH effect; Secondary structure; Tetanus neurotoxin

Secondary structure contents of tetanus neurotoxin have been estimated at neutral and acidic pH using circular dichroism (CD) and Fourier transform infrared (FT-IR) spectroscopy. An analysis of the far-ultraviolet CD spectra of the neurotoxin dissolved in 50 mM citrate-phosphate buffer (pH 7.0) revealed 20.0±2.1% α-helix, 50.5±2.1% β-pleated sheets, no β-turns, and 29.5% random coils, which is at considerable variance with results from an earlier detailed study of tetanus neurotoxin's secondary structures (J.P. Robinson, L.A. Holladay, J.H. Hash and D. Puett, J. Biol. Chem. 257 (1982) 407). However, the α-helix content estimated in this study is consistent with the earlier studies of Robinson et al. (J.P. Robinson, L.A. Holladay, J.B. Picklesimer and D. Puett, Mol. Cell. Biochem. 5 (1974) 147; J.P. Robinson, J.B. Picklesimer and D. Puett, J. Biol. Chem. 250 (1975) 7435) and with the study by Lazarovici et al. (P. Lazarovici, P. Yanai and E. Yavin, J. Biol. Chem. 262 (1986) 2645), although other secondary structural features do not agree with those of the previous studies. Secondary structure estimation from Fourier transform infrared spectra in both amide I and amide III frequency regions revealed 22–23% α-helix, 49–51% β-pleated sheets and 27–28% random coils, indicating a good correlation with the secondary structure content estimated from CD analysis. Lowering of the pH of the neurotoxin to 5.5 or 4.0 did not result in any noticeable change in the overall secondary structures. However, there were significant pH-induced variations observed in the individual curve-fitted FT-IR bands in the amide III frequency region. For example, the 1302 $cm^{-1}$ band (relative area, 4.2%) observed at pH 7.0 was shifted to 1297 $cm^{-1}$ (relative area, 2.2%) at pH 5.5, and the relative area of the band at 1316–1317 $cm^{-1}$ (α-helix) increased by approx. 40%. This study suggests that contrary to earlier reports, tetanus neurotoxin is a β-pleated sheet dominated structure, and although lower pH does not change the overall contents of the secondary structures, significant conformational alterations are observed.

## 1. Introduction

Tetanus neurotoxin is an extremely toxic protein ($MLD_{50} > 10^7$ per mg protein)produced by the anaerobic bacterium, *Clostridium tetani*. It is a high molecular weight protein ($M_r$ 150000) which acts on the presynaptic membranes of both central and peripheral nervous systems to block the release of certain neurotransmitters resulting in muscle paralysis [1–4]. The neurotoxin is synthesized as a single-chain protein that can be nicked at about one-third position from the N-terminus by endogenous proteases or by exogenous proteases such as trypsin [5]. The nicked form of neurotoxin consists of a light chain subunit (approx. 50 kDa) and a heavy chain subunit (approx. 100 kDa) linked through a disulfide bond(s) [5]. Studies of tetanus neurotoxin and its active fragments during the last two decades have enhanced

Correspondence address: B.R. Singh, Department of Food Microbiology and Toxicology, University of Wisconsin, 1925 Willow Drive, Madison, WI 53706, U.S.A.
* Present address: Centro C.N.R. Biomembrane Dipartimento di Science Biomediche, Universita' di Padova, Via Trieste, 35131 Padova, Italy.

knowledge of the cellular functions of the various domains of the protein (for recent reviews, see refs 4 and 6). However, the molecular mechanism of action of the tetanus neurotoxin is not yet known. In the proposed mode of action, the neurotoxin binds to the presynaptic membranes and the whole or a part of it is internalized into the cell through the bilayer membrane, where it causes a putative biochemical lesion(s) resulting in the blockage of the neurotransmitter release [4]. The binding and internalization steps involve the interaction of the neurotoxin with a non-polar lipid membrane which is known to change the conformation of the protein in terms of an increase in the $\alpha$-helix [7]. Therefore, the secondary structures could play significant roles in the function of the tetanus neurotoxin.

The amino acid sequence of the tetanus neurotoxin has been derived from the cloned nucleotide sequence [8,9]. However, the sequence has not provided any obvious clues about the structural basis of the neurotoxin action. For example, its hydropathy profile does not indicate any membrane-spanning domain with considerable hydrophobicity [8]. It has been recently proposed that amino acid residues in the protein segments having no significant hydrophobic index can be arranged in such a way as to provide amphiphilic structures in the secondary structural folding [10] so that compatible interactions with nonpolar domains of lipid bilayers can occur. Thus, the knowledge of secondary structure could be important in understanding the molecular mode of the neurotoxin's action.

The secondary structures of the tetanus neurotoxin have been analyzed in the past using far-ultraviolet circular dichroism (CD) [7,11–13]. However, the results have not been consistent in all the previous studies. For example, the $\alpha$-helix content varies from about 20% [7,11] to approx. 35% [13]. In addition, the random coil contents derived from far-ultraviolet CD spectra are estimated with an indirect method (i.e., % contents of $\alpha$-helix and $\beta$-sheets subtracted from 100%).

In this report, we have analyzed the secondary structures of the two-chain form of tetanus neurotoxin using Fourier transform infrared (FT-IR) and CD spectroscopy for $\alpha$-helix, $\beta$-sheets, $\beta$-turns and random coils. These results indicate that the secondary structures are significantly different from those reported in earlier studies in that they show a much higher content of ordered structures ($\sim$ 70%) in general, and $\beta$-pleated sheets in particular ($\sim$ 50%) which could be important for the understanding of the function of the neurotoxin.

Using an analogy with diphtheria toxin, it is believed that low pH-induced conformational changes in the neurotoxin facilitate the internalization of the tetanus neurotoxin inside the nerve cell (see 4). Therefore, we have investigated the effect of low pH on the conformation of the neurotoxin. The results indicate no major alteration in the overall secondary structure contents, although significant changes in the individual curve-fitted FT-IR bands were observed.

## 2. Materials and methods

Tetanus neurotoxin was isolated and purified from *Clostridium tetani* (strain Harvard Y-IV-3) according to the method of Ozutsumi et al. [14]. The purified neurotoxin was stored as ammonium sulfate precipitate at 4°C. For experiments, the precipitate was redissolved in 50 mM citrate-phosphate buffer (pH 7.0) and dialyzed against the same buffer to remove the trace amount of ammonium sulfate. As shown in fig. 1, the neurotoxin showed a single homogeneous band of 150 kDa on an 8–25% SDS-polyacrylamide electrophoresis gradient gel (SDS-PAGE). Upon reduction with mercaptoethanol, two bands corresponding to heavy ($\sim$ 100 kDa) and light ($\sim$ 50 kDa) chains were observed on the SDS-polyacrylamide gels, indicating that the neurotoxin was almost completely in the nicked form (fig. 1). The protein samples were filtered through a 0.2 $\mu$m filter (Gelman Sciences) before optical measurements. The chemicals used were of the highest grade available commercially. Buffers and solutions were prepared with deionized distilled water.

### 2.1. FT-IR measurements

The samples were analyzed on a Nicolet model 8210 FT-IR spectrometer which is equipped with

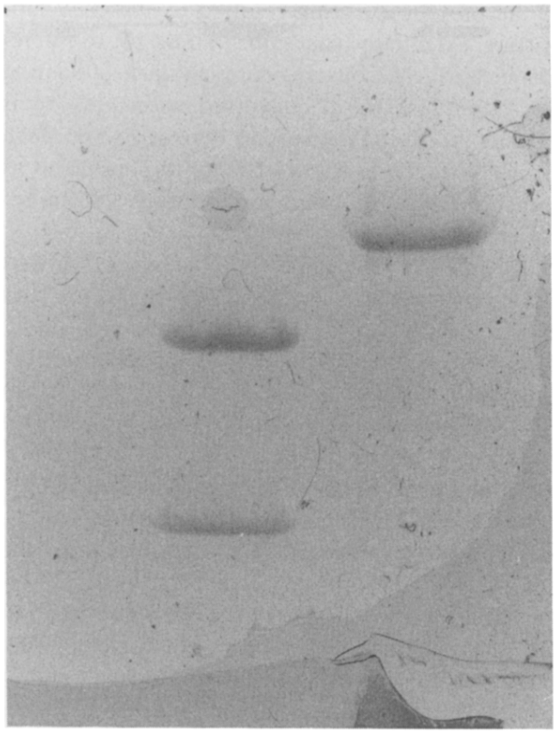

Fig. 1. SDS-polyacrylamide gel electrophoresis of the two-chain tetanus neurotoxin under non-reducing (right lane) and reducing (left lane) conditions on an 8–25% polyacrylamide gel.

a horizontal ATR (attenuated total reflectance) accessory containing a zinc selenide crystal. The data were collected using a room-temperature DTGS detector with an interferometer operating at 4 $cm^{-1}$ resolution with 256 scans co-added to produce each spectrum.

To record the FT-IR spectra, the neurotoxin at pH 7.0 was layered on the zinc selenide crystal and the spectrum was recorded. Then the bulk protein solution was replaced with 50 mM citrate-phosphate buffer (pH 7.0), and the spectrum of the adsorbed neurotoxin was recorded. In order to observe the effect of pH, the buffer of pH 7.0 was replaced by buffer of the desired pH after rinsing (two to three times) of the adsorbed neurotoxin with the latter. To obtain the final FT-IR spectra, the spectra of buffers of the corresponding pH values were subtracted as described below.

In each case, the absorbance spectrum of the buffer was used to eliminate the contribution of the strong water absorption at 1640 $cm^{-1}$ to the amide I band around 1650 $cm^{-1}$. This interference is eliminated by subtracting the spectrum of the buffer from that of the protein/buffer solution. Initially, some difficulty was experienced in selecting the proper scaling factor for this subtraction. If the 1640 $cm^{-1}$ water band is not properly subtracted, errors in the interpretation of the 1650 $cm^{-1}$ amide I band can occur. Accurate subtractions were obtained by varying the subtraction factor in an interactive manner until the broad water absorption around 800 $cm^{-1}$ was totally removed. Use of this region as the basis for the spectral subtraction of the buffer provides reliable and reproducible results.

After eliminating the interfering absorption due to the buffer, the spectrum of the protein remains. The amide I bands are typically only a few thousandths of an absorbance unit in intensity. In this study, all of the spectra were smoothed using a 9-point Savitsky-Golay algorithm to suppress the noise level prior to processing. The difference spectra were then multiplied by 100 to yield absorbances of a more convenient magnitude. The spectra were analyzed using the Nicolet FOCAS™ software package. This analysis proceeds in two steps. First, the spectral data are resolution enhanced during a Fourier self-deconvolution operation, and the peak positions in the enhanced spectrum are selected. In the second step, the peak widths, positions, intensities and percent Lorenntzian/Gaussian shape are varied to obtain the 'best' match to the original curve. The parameters are varied until the residual spectrum, obtained by subtracting the synthetic composite curve from the original data, is minimized. After the results are optimized, a table of all of the variable parameters, the synthetic composite curve, the difference spectrum obtained by subtracting the synthetic curve from the actual curve, the individual synthetic curves and the peak areas are available for interpretation. Second-derivative spectra were also used to support the Fourier self-deconvolution resolution enhancement results.

### 2.2. Circular dichroism

CD spectra of the tetanus neurotoxin samples were recorded on a modified Jasco J20 spectro-

polarimeter using essentially the same conditions as described earlier [15]. The instrument has been modified by interfacing it to an IBM personal computer in order to use Jasco J-500 software for data collection and processing. This interface allowed us to record several spectra of the same sample and average them out to enhance the signal-to-noise-ratio. The secondary structure composition values were estimated from the far-ultraviolet CD spectra using the method of Chang et al. [16]. The program for the secondary structure analyses was provided by Dr. C.S. C. Wu (University of California, San Francisco). For the recording of the ultraviolet CD spectra, protein concentrations in the range of 0.05–0.1 mg/ml were used in a 1 mm path length quartz curvette.

## 3. Results

### *3.1. FT-IR*

FT-IR spectra of the neurotoxin were recorded after allowing the protein to adsorb onto the surface of a zinc selenide crystal. The spectrum of adsorbed protein was first recorded while it was still exposed to the bulk protein solution. Subsequently, the bulk solution was replaced by the buffer (50 mM citrate-phosphate buffer, pH 7.0). There was no significant difference in the spectra of absorbed neurotoxin under the two conditions (fig. 2a and b), suggesting no alteration in the protein conformation upon adsorption to the surface of zinc selenide crystal. FT-IR spectra after subtraction of the water band show a single band at approx. 1650 $cm^{-1}$ (fig. 2b) with no resolution of the bands in this region of the spectrum. The positions and areas of these unresolved spectral bands are required for the secondary structure assignment. For this reason, self-deconvolution and second-order derivatization of the FT-IR spectra were carried out. Representative plots of deconvolved and derivatized spectra in the amide I frequency region are shown in fig. 2c and d, respectively. The deconvolution resolved bands at 1683, 1672, 1653, 1642, 1632 and at 1615 $cm^{-1}$ in the amide I frequency region of the spectrum of the neurotoxin. The second derivative of the protein spectrum resulted in evidence supporting essentially the same bands as those resolved by the deconvolution technique, indicating the validity of the deconvolved spectrum. As is evident in fig. 2, the second-derivative approach typically results in a lower signal-to-noise ratio as compared with the Fourier self-deconvolution approach.

In order to determine the contents of various secondary structures, we used a curve-fit analysis of the spectra to estimate the relative area under each band. Relative contents of secondary structures were derived as described in earlier studies [17,18]. The curve fitting of the spectrum revealed bands at 1678, 1653, 1642, 1633 and 1620 $cm^{-1}$ (fig. 3a) in the amide I frequency region (1700–1600 $cm^{-1}$). Fractional areas of these bands are listed in table 1. Based on the relative area, the 1653 $cm^{-1}$ band appears to be the most prominent followed by that at 1633 $cm^{-1}$. The band at 1653 $cm^{-1}$ could arise from both $\alpha$-helix and random coils [17–20]. The low-frequency band at 1633 $cm^{-1}$ arises due to $\beta$-pleated sheets [17,18,21,22]. The band at 1678 $cm^{-1}$ can be assigned to $\beta$-pleated sheets [17,18], although $\beta$-turns could also contribute at this frequency [23]. Because no characteristic bands for $\beta$-turns ($1671 \pm 3$ and $1683 \pm 2$ $cm^{-1}$ [17]) were observed, we believe that any contribution due to the overlapping band of $\beta$-turns is insignificant. The small band at 1642 $cm^{-1}$ could arise from $3_{10}$-helix. $\beta$-sheet or random coils [17,18]. The band observed at 1620 $cm^{-1}$ is most likely due to the Tyr side chain [24]. Based on these assignments and the relative areas of the assigned bands, the estimation of the secondary structures can be made as follows: $\alpha$-helix and unordered structure, 51%; $\beta$-pleated sheets, 49%.

The amide II frequency region (1600–1400 $cm^{-1}$) is not sensitive to the type of secondary structure conformations, and therefore, will not be described here. In the amide III frequency region, two major bands were observed at 1240 and 1314 $cm^{-1}$ (fig. 3b). A curve fit analysis resolved several small bands in this region as listed in table 2. Based on earlier infrared spectroscopic studies of proteins with known secondary structure [25], the bands in the amide III frequency region can be

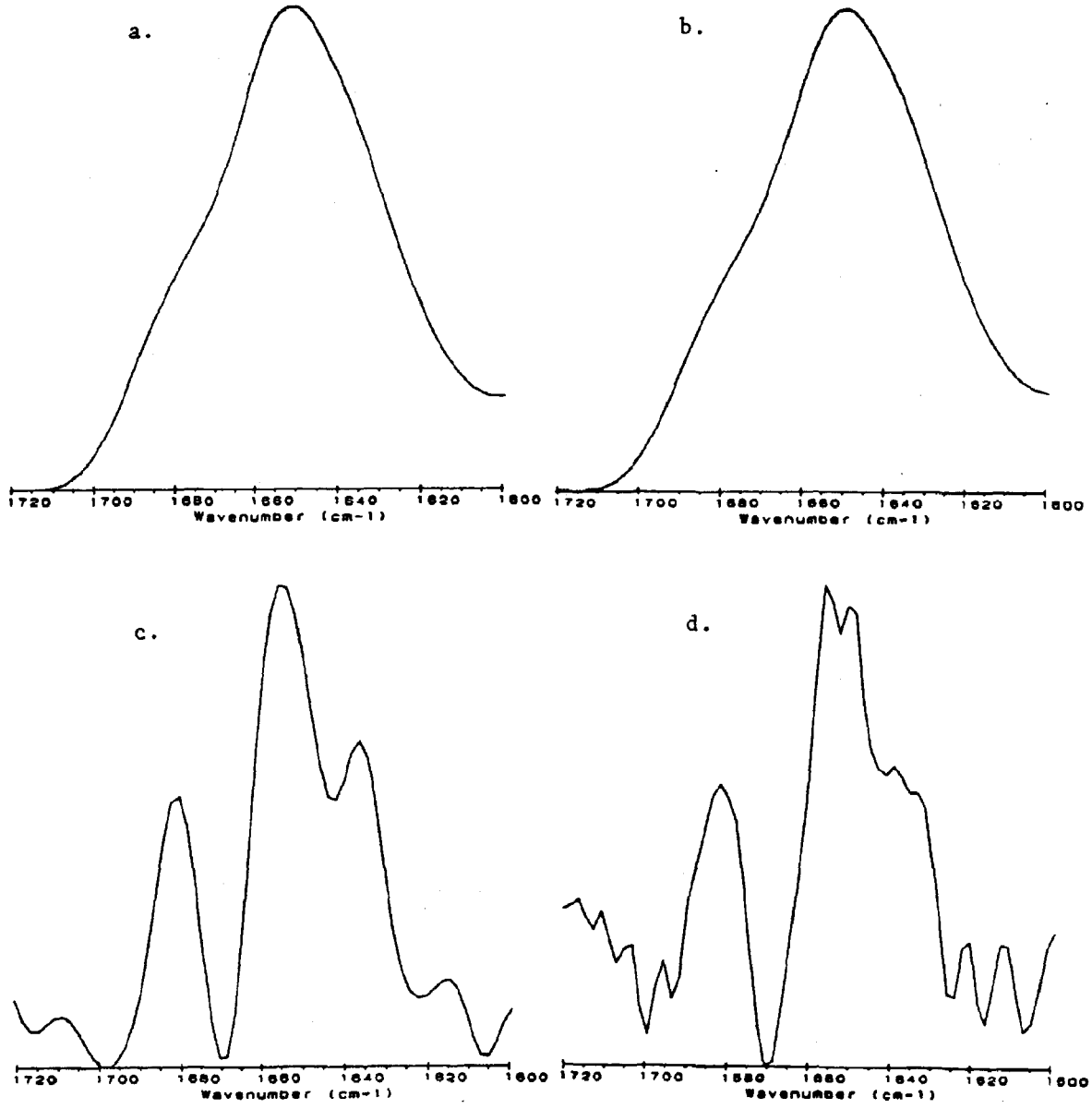


Fig. 2. FT-IR spectra of tetanus neurotoxin (a) in bulk solution; (b) adsorbed to Zn selenide crystal and exposed to 50 mM citrate-phosphate buffer (pH 7.0); (c) the spectrum in (b) after Fourier self-deconvolution; and (d) the spectrum in (b) after second-order derivatization. The spectra were recorded at room temperature (23–25 °C) as described in section 2.

assigned as follows: 1317–1280 $cm^{-1}$, $\alpha$-helix; 1271–1245 $cm^{-1}$, unordered structures; 1245–1230 $cm^{-1}$, $\beta$-pleated sheets. In view of the above assignments, tetanus neurotoxin appears to have 22% $\alpha$-helix, 33–51% $\beta$-pleated sheets and 27–45% unordered structures (table 2).

pH-induced changes in the neurotoxin structure were studied by FT-IR spectroscopy. The neuro-

toxin adsorbed to the zinc selenide crystal was first exposed to pH 7.0 buffer as discussed above. In order to record the spectrum at another pH, the buffer of pH 7.0 was replaced by buffer of a given pH, and spectra were recorded after 5 min incubation. Fig. 4 shows FT-IR spectra of the adsorbed neurotoxin exposed to 50 mM citrate-phosphate buffer (pH 5.5). In the amide I frequency region (fig. 4a), a curve-fit analysis revealed bands at 1679, 1652, 1642, 1631 and 1620 $cm^{-1}$ (table 1).

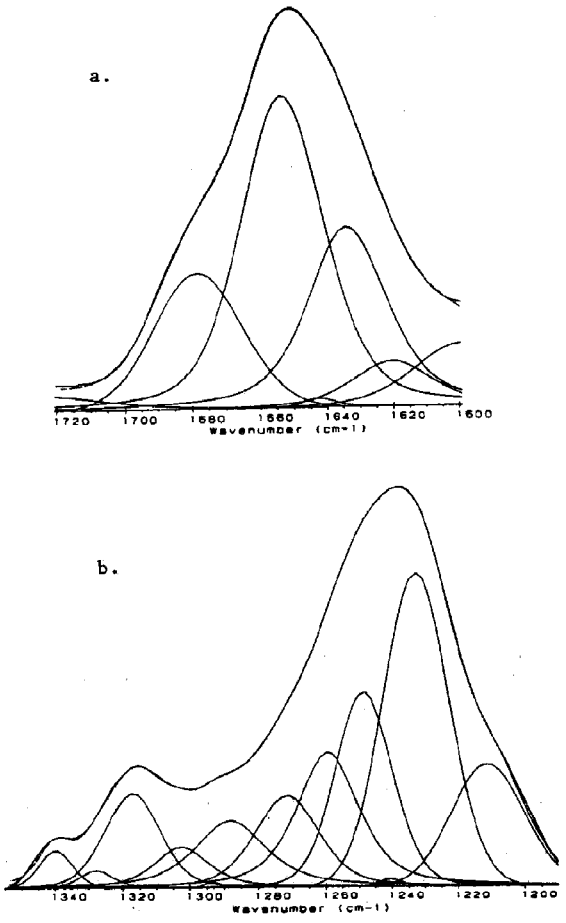


Fig. 3. Curve-fitted FT-IR spectra of tetanus neurotoxin dissolved in 50 mM citrate-phosphate buffer (pH 7.0), in amide I (a) and amide III (b) frequency regions. Upper spectra in both frequency regions show the actual recorded spectra of the neurotoxin adsorbed to Zn selenide crystal and the synthetic spectra obtained form the addition of the constituent spectra resolved after curve fitting. Differences between the recorded and synthetic spectra were almost non-existent.

Table 1

Spectral band positions and fractional areas of amide I bands of tetanus neurotoxins at different pH values

| pH | Band position ($cm^{-1}$) | Band area (%) | Assignment [a] |
|---|---|---|---|
| 7.0 | 1678 | 20 (22) [b] | β-sheets |
| | 1653 | 50 (48) | α-helix and random coil |
| | 1642 | 1 (2) | α-helix, β-sheet, random coil |
| | 1633 | 29 (28) | β-sheet |
| | 1620 | – | Tyr [c] |
| 5.5 | 1679 | 17 (16) | β-sheets |
| | 1652 | 51 (52) | α-helix and random coil |
| | 1641 | 4 (3) | α-helix, β-sheet, random coil |
| | 1631 | 28 (29) | β-sheet |
| | 1620 | – | Tyr [c] |
| 4.0 | 1679 | 21 (19) | β-sheets |
| | 1652 | 51 (53) | α-helix and random coil |
| | 1640 | 0 (1) | α-helix, β-sheet, random coil |
| | 1633 | 28 (27) | β-sheet |
| | 1620 | – | Tyr [c] |

[a] See text for band assignments.
[b] Numbers in parentheses are results from a set of repeat measurements.
[c] Band at 1620 $cm^{-1}$ is assigned to Tyr residues and is therefore not included in the relative area calculations.

The estimation of secondary structure contents of the neurotoxin at pH 5.5, based on band assignments and relative areas (vide supra), did not show any change as compared with the pH 7.0 analysis (α-helix and unordered structures, 51%; β-pleated sheets, 45–49%; table 1). In the amide III frequency region (fig. 4b), the curve-fit analysis indicated most of the same bands observed at pH 7.0 (table 2). However, there were some notable differences in band positions and their relative areas. For example, the relative area of the 1317 $cm^{-1}$ band at pH 7.0 was 8.7% whereas at pH 5.5, it was 13.0% (table 2). The band at 1303 $cm^{-1}$ (at pH 7.0) was shifted to 1297 $cm^{-1}$ along with a decrease in its relative area. The overall contents of secondary structures of the neurotoxin at pH 5.5 based on the analysis of the amide III frequency region (vide supra) indicated slightly increased α-helical content (25%; table 2).

Exposure of the adsorbed neurotoxin (already exposed to pH 5.5 buffer) to pH 4.0 did not introduce any noticeable alterations in the FT-IR

spectra, either in the amide I or amide III frequency regions (fig. 5) except for variations in the relative areas of spectral bands (tables 1 and 2). The secondary structure contents were 51% α-helix + unordered structures, and 49% β-pleated sheets, as derived from the amide I frequency bands (table 1). Based on the amide III frequency bands, secondary structure contents were estimated at 19% α-helix, 31–50% β-pleated sheets and 30–50% unordered structures (table 2).

In addition to the assigned FT-IR spectral bands in the amide III frequency region (table 2), we observed a band at 1211 $cm^{-1}$ at pH 7.0 (fig. 3b). At pH 5.5, two bands appeared at 1223 and 1204 $cm^{-1}$ (fig. 4b) with relative areas of 15.1 and 1.9%, respectively. Lowering the pH to 4.0 (fig. 5b) caused a further increase in the low-frequency band at 1208 $cm^{-1}$ (with a relative area of 7.1%, whereas the band at 1223 remained more or less constant (relative area of 13.8%).

Table 2

FT-IR spectral bands and fractional areas of amide III region of the tetanus neurotoxin at different pH values

| pH | Band position ($cm^{-1}$) | Band area (%) | Assignment [a] |
|---|---|---|---|
| 7.0 | 1317 | 8.7 (9.3) [b] | α-helix |
| | 1302 | 4.2 (3.7) | α-helix |
| | 1293 | 0.1 (0.1) | α-helix |
| | 1288 | 9.4 (9.8) | α-helix |
| | 1272 | 10.4 (11.2) | unordered |
| | 1259 | 16.4 (15.6) | unordered |
| | 1247 | 18.3 (18.5) | β-sheet/unordered |
| | 1241 | 0.3 (0.2) | β-sheet |
| | 1232 | 32.2 (31.6) | β-sheet |
| 5.5 | 1316 | 13.0 (12.2) | α-helix |
| | 1297 | 2.2 (2.4) | α-helix |
| | 1287 | 10.0 (10.6) | α-helix |
| | 1268 | 13.5 (12.7) | unordered |
| | 1257 | 14.5 (15.3) | unordered |
| | 1247 | 18.2 (19.0) | β-sheet/unordered |
| | 1237 | 28.5 (27.8) | β-sheet |
| 4.0 | 1316 | 6.2 (6.1) | α-helix |
| | 1302 | 2.9 (3.3) | α-helix |
| | 1293 | 3.5 (3.1) | α-helix |
| | 1284 | 6.2 (6.7) | α-helix |
| | 1272 | 12.3 (11.8) | unordered |
| | 1258 | 17.3 (18.1) | unordered |
| | 1248 | 20.6 (19.9) | β-sheet/unordered |
| | 1236 | 30.8 (31.0) | β-sheet |

[a] Based on the studies of Kaiden et al. [25].
[b] Numbers in parentheses are the results of an independent set of measurements.

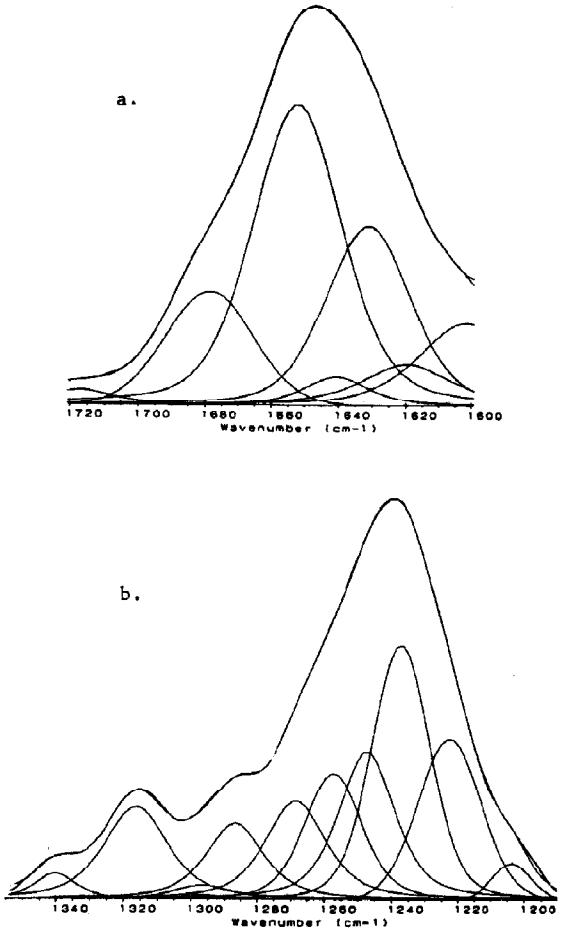


Fig. 4. Curve-fitted FT-IR spectra of tetanus neurotoxin dissolved in 50 mM citrate-phosphate buffer (pH 5.5), in amide I (a) and amide III (b) frequency regions. Other details are as given in fig. 3.

### 3.2. Circular dichroism

CD spectra of the neurotoxin dissolved in 50 mM citrate-phosphate buffer, (pH 7.0) were recorded between 190 and 250 nm for the estimation of secondary structures using the method of Chang et al. [16]. The far-ultraviolet CD spectrum (fig. 6) showed a shallow double-well-shaped structure

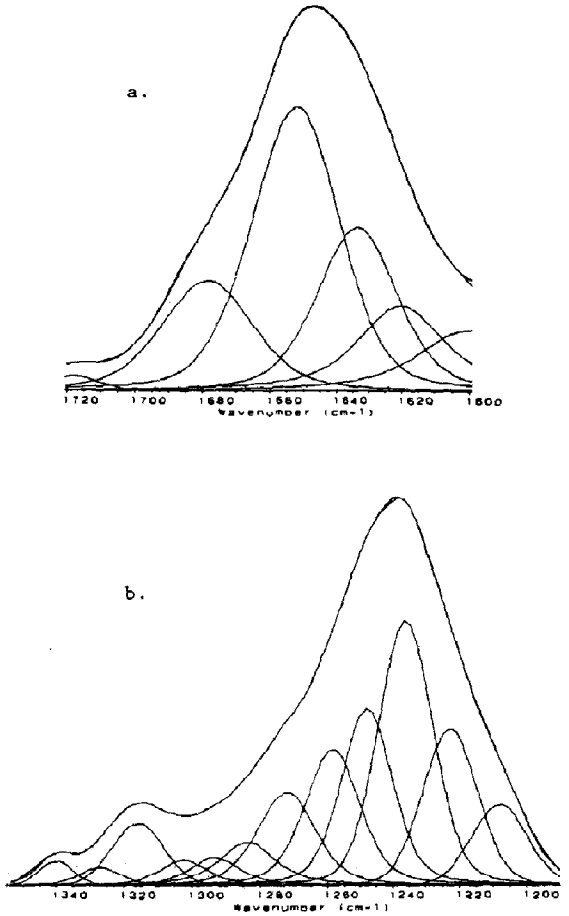


Fig. 5. Curve-fitted FT-IR spectra of tetanus neurotoxin dissolved in 50 mM citrate-phosphate buffer (pH 4.0), in amide I (a) and amide III (b) frequency regions. Other details are as given in fig. 3.

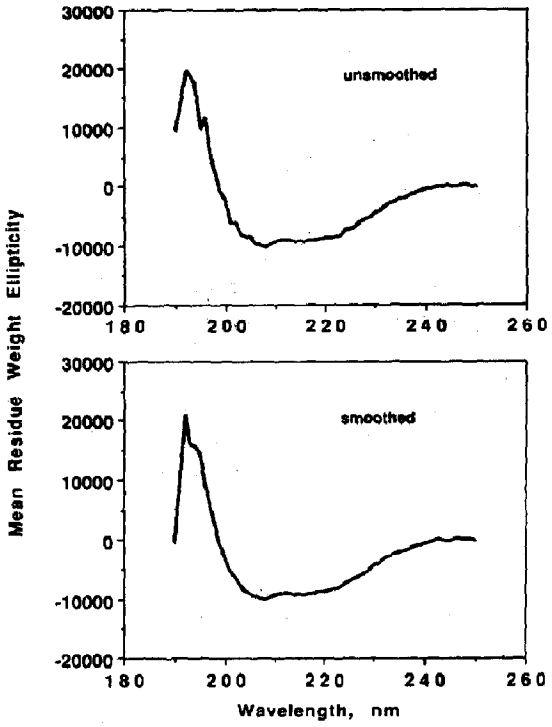


Fig. 6. Smoothed (a 5-point smoothing at 0.2-nm intervals) and non-smoothed CD spectra of tetanus neurotoxin dissolved in 50 mM citrate-phosphate buffer (pH 7.0). The spectra are the average of five recordings at room temperature (23–25 °C) using a 1 mm path length quartz curvette.

with negative bands at 216 and 208 nm. A sharp positive CD signal was observed at 192 nm. The mean residue weight ellipticities were −9300, −10100 and 20800 degree $cm^2$ $dmol^{-1}$, respectively, at 216, 208 and 192 nm. The secondary structural contents derived from the CD data (table 3) was revealed as 20.0% α-helix, 50.5% β-pleated sheets, no β-turns, and 29.5% random coils.

Table 3

Secondary structural analysis of tetanus neurotoxin dissolved in 50 mM citrate-phosphate buffer (pH 7.0) derived from the ultraviolet CD spectrum and FT-IR spectra in the amide I and III frequency regions

| Secondary structure | CD analysis [a] (%) | FT-IR analysis [b] (%) |
|---|---|---|
| α-Helix | 20.0 ± 2.1 | 22–23 |
| β-Pleated sheets | 50.5 ± 2.1 | 49–51 |
| β-Turns | 0.0 | 0.0 |
| Random coils | 29.5 ± 0.0 | 26–27 |

[a] Apparent secondary structure contents were estimated based on the method of Chang et al. [16] by using the mean residue ellipticities at 1-nm intervals between 240 and 190 nm. The values are the average of two independent sets of experiments.

[b] Secondary structure contents derived from tables 1 and 2. See text for the basis of the estimation.

## 4. Discussion

Water is a strong infrared absorber. If quantitative measurements are desired, the effective path length of the sample must be about 15–40 $\mu$m so that the interfering water absorption can be properly eliminated. In order to explore the effect of varying matrices on the protein spectra, it is necessary somehow to immobilize the protein. The ATR technique has been shown to be a viable method for this type of experiment for two reasons. First, by its very nature the ATR technique allows short optical path lengths [26]. Second, when a solution of a protein is placed in contact with the ATR crystal, a layer becomes adsorbed on the crystal surface. This allows the matrix to be modified without removing the protein [22]. For example, to observe the effect of pH on tetanus neurotoxin, buffer of a given pH was layered on top of the neurotoxin adsorbed on the crystal surface.

The model 8210 along with its horizontal ATR accessory was selected as the instrument of choice for the experiments although there are many reports involving the analysis of aqueous solutions using the Circle Cell™ ATR accessory unit manufactured by Spectra-Tech used in conjunction with a general-purpose FT-IR spectrometer. In our experience, there are several problems associated with the use of the Circle Cell™ accessory for the analysis of protein solutions. The crystal of the Circle Cell™ accessory is cylindrical and runs down the center of a hollow stainless cell tube. In the case of the sealed version, the sample is passed into the cell using plastic tubing. With this type of configuration it is necessary to dismantle and clean the cell between experiments in order to remove totally the adsorbed protein. A second common problem is that of a water vapor mismatch. Most FT-IR spectrometers are purged with dry air or nitrogen to eliminate absorptions due to atmospheric water vapor. With a standard FT-IR instrument it is difficult to obtain spectra without trace absorptions due to water. Any residual absorptions due to water would seriously affect the analysis of the amide I protein band. The Nicolet 8210 is a sealed and desiccated instrument and as a result residual absorptions due to water vapor are eliminated.

The secondary structure estimations of the tetanus neurotoxin carried out earlier have not resolved the inconsistency in the results [7,11–13]. Two main reasons are perhaps responsible for the considerable inconsistency in the secondary structure estimation by previous workers. First, the far-ultraviolet CD spectra used for deriving the contents of the secondary structures were recorded only to a minimum of 200 nm, although CD signals to 175 nm are known to be affected by the secondary structural conformation of the peptide backbone [16,27–29]. Second, most of the earlier studies did not use any comprehensive programs based on sufficient reference CD spectra of proteins with known secondary structures. In this study, we have used CD spectra between 240 and 190 nm for the secondary structure analysis using the method of Chang et al. [16]. In this method, the apparent secondary structures of a given protein are estimated by a linear least-square analysis of the CD spectra of 15 reference proteins of known structures by X-ray analysis of the crystallographic structures [16]. Additionally, we have used a relatively novel technique of FT-IR spectroscopy as an independent and complementary method to analyze the secondary structures of the tetanus neurotoxin.

The $\alpha$-helical content of 20% estimated in this study (table 3) agrees well with earlier studies [7,11,12], but not with the latest estimation of 35% $\alpha$-helix by Robinson et al. [13]. Since in the latter study, the same set of protein CD reference spectra were used as in the present study, the differences could arise mainly due to the smaller data points used by Robinson et al. [13], i.e., they used the CD signals between 240 and 200 nm whereas we have used those between 240 and 190 nm (fig. 6). The peptide backbones in different conformations differ considerably in their CD signals between 200 and 190 nm [30,31]. The estimated $\beta$-pleated sheet structures (50.5%, table 3) of the tetanus neurotoxin in this study are much higher than those in previously reported results (18–30% [11–13]). The discrepancy could again be explained by the factors listed for the difference in $\alpha$-helical contents (vide supra). In the present analysis, no $\beta$-turns were observed (table 3), although it is unlikely that a globular protein of

approx. 150 kDa is devoid of any turns or bends. The secondary structure predicted from the primary amino acid sequence of the tetanus neurotoxin using the method of Chou and Fasman [32] revealed 16.3% $\alpha$-helix, 29.1% $\beta$-pleated sheets, 41.5% $\beta$-turns and 13.1% random coils. From the predicted results, $\alpha$-helical contents match reasonably well with the experimental results in this study. However, the predicted data indicates a very high content of $\beta$-turns that were not observed in the experimental CD data. The discrepancy could arise from the inherent inaccuracies in the programs used to determine secondary structures [16,32,33]. The absence of $\beta$-turns estimated from the CD spectra could arise from the limitations of the method in estimating the $\beta$-turns, as pointed out by Chang et al. [16]. However, FT-IR spectra of the neurotoxin also did not indicate any noticeable vibrational bands corresponding to the $\beta$-turns (vide infra). Therefore, it seems that tetanus neurotoxin does not contain any significant amount of $\beta$-turns.

Curve-fit analysis of the FT-IR spectra in the amide I frequency region and the derived estimation of the secondary structure contents provided a clear estimation of $\beta$-pleated sheets ($\sim$ 49%, table 1), because the 1633 and 1678 $cm^{-1}$ bands can unequivocally be assigned to the $\beta$-pleated sheets [17,18,21]. This estimation is quite consistent with the estimation of $\beta$-pleated sheets from the far-ultraviolet CD spectra (table 3). The $\alpha$-helical content could not be derived unequivocally from the 1653 $cm^{-1}$ band (fig. 2 and table 1) because this band can have a contribution from vibrational modes of N-H in both the $\alpha$-helical conformation as well as in the unordered structures [17,19,20,23], although the 1650 $cm^{-1}$ band has been used by other workers to estimate only $\alpha$-helix [18]. Since the secondary structures estimated from the far-ultraviolet CD data (this as well as previous studies) and from the primary structure show considerably smaller amount of $\alpha$-helix than would be estimated from the 1653 $cm^{-1}$ band (51% relative area), we decided to analyze the FT-IR spectra in the amide III frequency region which has been effectively used for assigning $\alpha$-helix and unordered structures [23,25].

The presence of a prominent band at 1240 $cm^{-1}$ relative to that at 1317 $cm^{-1}$ indicated the presence of a significant amount of unordered structures in the polypeptide folding of the neurotoxin. The estimated $\alpha$-helical content of 22.4% is quite consistent with the CD analysis (table 3) and confirms the fact that the 1653 $cm^{-1}$ band has contributions from both $\alpha$-helix and unordered structures. This should leave about 28 (51%–22.4%) of the peptide segments in unordered structures which is also consistent with far-ultraviolet CD data (table 3). However, based on the relative areas of amide III frequency bands corresponding to unordered structures (1270–1245 $cm^{-1}$ [25]), the estimated unordered structures were approx. 45% (table 2). This estimation includes the band at 1247 $cm^{-1}$ which is a lower limit for the assignments of unordered structures [25]. Below 1245 $cm^{-1}$ and up to 1230 $cm^{-1}$, the bands are assigned to $\beta$-pleated sheets [25]. Therefore, the 1247 $cm^{-1}$ can be assigned to $\beta$-pleated sheets, especially in view of the observation that the $\beta$-sheet amide III vibration band at about 1238 $cm^{-1}$ can split into 1233 and 1245 $cm^{-1}$ components [22]. In this way, the amount of $\beta$-pleated sheets can be estimated to be approx. 51%. This estimation is not only consistent with that of $\beta$-pleated sheets from the amide I frequency region (table 1), but also that from the far-ultraviolet CD spectra (table 3). The amount of unordered structures, thus, remains at about 27% which is consistent with the CD analysis (29.5%).

Lowering the pH to 5.5 (fig. 4) or to 4.0 (fig. 5) did not cause any noticeable change in the FT-IR spectra of the amide I frequency region (table 1), indicating no alterations in the overall composition of secondary structures. However, this does not rule out any secondary structural change in specific domains of the polypeptide segment. A small increase in the $\alpha$-helical content at pH 5.5 (table 2) is probably an indication of such alteration, although overall secondary structure contents remained similar at three pH values studied based on the amide I frequency region. It is important to note that individual relative areas of bands (in the amide III frequency region) assigned to a specific secondary structural conformation (e.g., $\alpha$-helix) varied significantly (table 2). This

supports the idea of alterations in the secondary structural folding of the neurotoxin at lower pH values even though overall contents remained unchanged. Additionally, we observed two different bands appearing at a lower frequency in the amide III region (1223 and 1203–1206 $cm^{-1}$) at pH 5.5 and 4.0 that were not observed at pH 7.0. The relative area of the band at 1203–1206 $cm^{-1}$ showed a progressive increase with decrease in pH from 7.0 to 4.0 (figs 3–5). Although it is not possible to assign these bands to any specific conformations, their appearance at low pH reflects a change in the protein conformation. The pH-induced secondary structure changes are similar to those observed for diphtheria toxin [34], where overall secondary structures of the toxin remained essentially the same at pH 7.3 and at pH 4.0, but individual curve-fitted bands showed variations. Thus, the present study is significant for it suggests that the analogy of diphtheria for the molecular mode of tetanus action may be well founded.

The secondary structures of tetanus neurotoxin estimated in this study are similar to those of a related group of neurotoxins, botulinum [35,36] which contain approx. 20% $\alpha$-helix and approx. 45% $\beta$-pleated sheets. Tetanus and botulinum neurotoxins share some of their pharmacological characteristics [4], and have significant sequence homology [37]. It is believed that tetanus and botulinum neurotoxins have similar modes of action for blocking the neurotransmitter release [4]. Therefore, the similarity in the secondary structure contents may have significance for the molecular mode of the neurotoxin action. Low pH is known to induce the channel-forming activity of both tetanus and botulinum neurotoxins (cf. ref. 4), and thus, the changes in the structure of the neurotoxins may provide a basis for understanding the mechanism of their action at the molecular level. The present report is the first study to analyze the secondary structure of tetanus neurotoxin in detail using two different techniques (CD and FT-IR spectra), and to analyze low pH-induced changes.

In conclusion, the present data suggest that (i) the tetanus neurotoxin is a high $\beta$-pleated sheet containing protein with low $\alpha$-helix content, contrary to earlier reports; (ii) very low $\beta$-turn contents are present in the neurotoxin as revealed by both CD and FT-IR spectra; (iii) about 70% of the tetanus neurotoxin has ordered structure; (iv) the secondary structure contents of tetanus neurotoxin are similar to a functionally related botulinum neurotoxin; (v) low pH does not change the overall secondary structures, but changes in the conformation are noticeable based on the amide III frequency region of FT-IR spectra.

## Acknowledgements

This study was partly supported by a small grant from Nicolet Instrument Corp. to B.R.S. We thank Dr. R. Rappuoli (Sclavo Research Center) for providing the *C. tetani* cultures. G.S. wishes to thank Dr. Montecucco for support.

## References

1 B. Bizzini, Microbiol. Rev. 43 (1979) 224.
2 H. Bigalke and E. Habermann, Naunyn Schmiedeberg's Arch. Pharmacol. 312 (1980) 255.
3 H.H. Wellhöner, Rev. Physiol. Biochem. Pharmacol. 93 (1982) 1.
4 L.L. Simpson, Annu. Rev. Pharmacol. Toxicol. 26 (1986) 427.
5 M. Matsuda, in: Botulinum neurotoxin and tetanus toxin, ed. L.L. Simpson (Academic Press, Sandiego, 1989) p. 69.
6 L.L. Simpson, Botulinum neurotoxin and tetanus toxin (Academic Press, San Diego, 1989).
7 P. Lazarovici, P. Yanai and E. Yavin, J. Biol. Chem. 262 (1987) 2645.
8 U. Eisel, W. Jarausch, K. Goretzki, A. Henschen, J. Engles, U. Weller, M. Hudel, E. Habermann and H. Niemann, EMBO J. 5 (1986) 2495.
9 N.F. Fairweather and V.A. Lyness, Nucleic Acids Res. 14 (1986) 7809.
10 H. Niemann, B.A. Beckh, T. Binz, U. Eisel, S. Demotz, T. Mayer and C. Widman, in: Bacterial protein toxins, eds. F.J. Fehrenbach, J.E. Alouf, P. Falmagne, W. Goebel, J. Jljaszewicz, D. Jürgens and R. Rappuoli (Gustav Fischer, Stuttgart, 1988) p. 29.
11 J.P. Robinson, L.A. Holladay, J.B. Picklesimer and D. Puett, Mol. Cell. Biochem. 5 (1974) 147.
12 J.P. Robinson, J.B. Picklesimer and D. Puett, J. Biol. Chem. 250 (1975) 7435.
13 J.P. Robinson, L.A. Holladay, J.H. Hash and D. Puett, J. Biol. Chem. 257 (1982) 407.

14 K. Ozutsumi, N. Sugimoto and M. Matsuda, Appl. Environ. Microbiol. 49 (1985) 939.
15 B.R. Singh and M.J. Betley, J. Biol. Chem. 264 (1989) 4404.
16 C.T. Chang, C.S.C. Wu and J.T. Yang, Anal. Biochem. 91 (1978) 13.
17 H. Susi and D.M. Byler, Methods Enzymol. 130 (1986) 290.
18 P.W. Holloway and H.H. Mantsch, Biochemistry 28 (1989) 931.
19 S. Krimm, J. Mol. Biol. 4 (1962) 528.
20 H. Susi, S.N. Timasheff and L. Stevens, J. Biol. Chem. 242, (1967) 5460.
21 J.M. Olinger, D.M. Hill, R.J. Jakobsen and R.S. Brody, Biochim. Biophys. Acta 869 (1986) 89.
22 R.J. Jakobsen and F.M. Wasacz, in: Proteins at interfaces: Physicochemical and biochemical studies, eds. J.L. Brash and T.A. Horbett (American Chemical Society, 1987) p. 339.
23 F.M. Wasacz, J.M. Olinger and R.J. Jakobsen, Biochemistry 26 (1987) 1464.
24 W.K. Surewicz, A.G. Szabo and H.H. Mantsch, Eur. J. Biochem. 167 (1987) 519.
25 K. Kaiden, T. Matsui and S. Tanaka, Appl. Spectrosc. 41 (1987) 180.
26 N.J. Harrick, Internal reflection spectroscopy (Harrick Scientific, Ossining, NY, 1979) 2nd edn.
27 J.P. Hennessey, Jr and C.A. Johnson, Biochemistry 20 (1981) 1085.
28 L.A. Compton and C.A. Johnson, Anal Biochem. 155 (1986) 155.
29 J.T. Yang, C.S.C. Wu and H.M. Martinez, Methods Enzymol. 130 (1986) 208.
30 N. Greenfield and G.D. Fasman, Biochemistry 8 (1969) 4108.
31 I.P. Saxena and D.B. Wetlaufer, Proc. Natl. Acad. Sci. U.S.A. 68 (1971) 969.
32 P.Y. Chou and G.D. Fasman, Annu. Rev. Biochem. 47 (1978) 251.
33 S.D. Black and J.C. Glorioso, Biotechniques 4 (1985) 448.
34 V. Cabiaux, E. Goormaghtigh, R. Wattiez, P. Falmgne and J.M. Ruysschaert, Biochimie 71 (1989) 153.
35 B.R. Singh and B.R. DasGupta, Mol. Cell. Biochem. 85 (1989) 67.
36 B.R. Singh and B.R. DasGupta, Mol. Cell. Biochem. 86 (1989) 87.
37 T. Binz, U. Eisel, H. Kurazono, T. Binschek, H. Bigalke and H. Niemann, in: Bacterial protein toxins, eds. R. Rappuoli, J.E. Alouf, J. Freer, F.J. Fehrenbach, P. Falmagne and C. Montecucco (Gustav Fischer, Stuttgart, 1990) in the press.